GLOBAL VERY LONG BASELINE INTERFEROMETRY OBSERVATIONS OF THE 6.0 GHz HYDROXYL MASERS IN ONSALA 1

Citation: Fish, Vincent L., and Loránt O. Sjouwerman. "GLOBAL VERY LONG BASELINE INTERFEROMETRY OBSERVATIONS OF THE 6.0 GHz HYDROXYL MASERS IN ONSALA 1." The Astrophysical Journal 716, no. 1 (May 13, 2010): 106–113. © 2010 American Astronomical Society.

As Published: http://dx.doi.org/10.1088/0004-637x/716/1/106

Publisher: Institute of Physics/American Astronomical Society

Persistent URL: http://hdl.handle.net/1721.1/96121

Version: Final published version: final published article, as it appeared in a journal, conference proceedings, or other formally published context

The Astrophysical Journal, 716:106–113, 2010 June 10 doi:10.1088/0004-637X/716/1/106

GLOBAL VERY LONG BASELINE INTERFEROMETRY OBSERVATIONS OF THE 6.0 GHz HYDROXYL MASERS IN ONSALA 1

Vincent L. Fish[1] and Loránt O. Sjouwerman[2]
[1] MIT Haystack Observatory, Route 40, Westford, MA 01886, USA; vfish@haystack.mit.edu
[2] National Radio Astronomy Observatory, 1003 Lopezville Road, Socorro, NM 87801, USA; lsjouwer@nrao.edu
Received 2010 March 10; accepted 2010 April 20; published 2010 May 13

ABSTRACT

We present global very long baseline interferometry observations of the first excited-state hydroxyl (OH) masers in the massive star-forming region Onsala 1 (ON 1). The 29 masers detected are nearly all from the 6035 MHz transition and nearly all are identifiable as Zeeman pair components. The 6030 and 6035 MHz masers are coincident with previously published positions of ground-state masers to within a few milliarcseconds, and the magnetic fields deduced from Zeeman splitting are comparable. The 6.0 GHz masers in ON 1 are always found in close spatial association with 1665 MHz OH masers, in contrast to the situation in the massive star-forming region W3(OH), suggesting that extreme high density OH maser sites (excited-state masers with no accompanying ground-state maser, as seen in W3(OH)) are absent from ON 1. The large magnetic field strength among the northern, blueshifted masers is confirmed. The northern masers may trace an outflow or be associated with an exciting source separate from the other masers, or the relative velocities of the northern and southern masers may be indicative of expansion and rotation. High angular resolution observations of nonmasing material will be required in order to understand the complex maser distribution in ON 1.

Key words: ISM: individual objects (ON 1) – ISM: magnetic fields – masers – radio lines: ISM – stars: formation

Online-only material: color figures

1. INTRODUCTION

Onsala 1 (ON 1) is a kinematically complex site of massive star formation. In the 1.6 and 6.0 GHz transitions of hydroxyl (OH), masers are seen in two disjoint velocity ranges: −2 to +6 km s^{-1} in the north of the source and +11 to +16 km s^{-1} projected atop and to the south of the H II region (Argon et al. 2000; Fish et al. 2005; Nammahachak et al. 2006; Fish 2007; Fish & Reid 2007). A 4765 MHz excited-state maser at +24.1 km s^{-1} was also reported by Gardner & Martin-Pintado (1983) but never redetected. The highly excited 13,441 MHz transition shows similar velocity structure as the 1.6 and 6.0 GHz masers (Baudry & Desmurs 2002; Fish et al. 2005), although an interferometric map of the 13 GHz masers has not yet been published. The systemic velocity of the H II region as measured by Zheng et al. (1985) in H76α emission is approximately +5 km s^{-1}, which led the authors to conclude that the redshifted masers seen atop the H II region are undergoing infall. However, recent proper motion measurements strongly suggest that the masers are tracing slow (∼5 km s^{-1}) expansion in ON 1 (Fish & Reid 2007), similar to what is seen in W3(OH) (Bloemhof et al. 1992; Wright et al. 2004a; Fish & Sjouwerman 2007).

The ground-state OH masers in ON 1 have been observed with connected element interferometry (Ho et al. 1983; Argon et al. 2000; Nammahachak et al. 2006; Green et al. 2007) and with very long baseline interferometry (VLBI; Fish et al. 2005; Fish & Reid 2007) on multiple occasions. However, the only VLBI observations of the excited-state 6.0 GHz masers were taken by Desmurs & Baudry (1998) with a three-station array. Due to the poor image fidelity inherent with such a sparse array, they were only able to detect seven masers at 6035 MHz and two at 6030 MHz, ranging in flux density from 0.5 to 7.1 Jy. The large increase in the number of telescopes with 6.0 GHz capability has since made high-fidelity imaging of northern 6.0 GHz maser sources possible.

A prime motivation for observing ON 1 with a high sensitivity, high angular resolution, high spectral resolution VLBI array derives from the experience observing W3(OH), another nearby massive star-forming region. In W3(OH), it was found that the 6030 and 6035 MHz OH masers traced some areas where no ground-state masers have been observed and highlighted portions of other areas where ground-state masers are abundant, allowing a greater understanding of the large-scale (Galactic cloud) structure delineated by molecules in the source (Fish & Sjouwerman 2007). Of the massive star-forming regions visible from the north, ON 1 is one of the brightest 6.0 GHz OH maser sources, with numerous masers detected in the Baudry et al. (1997) survey. Thus, in addition to being an interesting source per se, ON 1 is also an interesting test case to determine to what degree OH masers in the first excited state can provide information not available from the ground-state masers alone.

2. OBSERVATIONS AND DATA REDUCTION

ON 1 was observed on 2008 June 15 with a global array consisting of two National Radio Astronomy Observatory (NRAO) and seven European VLBI Network (EVN) telescopes with $\lambda = 5$ cm capability (experiment code GS029). The participating stations were Effelsberg, the Green Bank Telescope (GBT), a single Expanded Very Large Array (EVLA) telescope, Hartebeesthoek, Jodrell Bank (Mark 2), Medicina, Onsala (85 ft), Toruń, and Westerbork (single telescope).

Both the 6030.747 and 6035.092 MHz main-line transitions of the first excited state ($^2\Pi_{3/2}$, $J = 5/2$) of OH were observed in dual circular polarization mode. For each transition, a 500 kHz bandwidth (24.8 km s^{-1}) was centered at an LSR velocity of +8 km s^{-1} in order to cover the full range of velocities of maser emission previously detected in ON 1. At correlation time, the data were accumulated for 1 s intervals and channelized into 512 spectral channels, corresponding to a spacing of 0.049 km s^{-1}.

Table 1
Detected Masers at 6030 and 6035 MHz

Pol.	v_{LSR} (km s^{-1})	R.A. Offset (mas)	Decl. Offset (mas)	Flux Density (Jy)	Δv (km s^{-1})	Gradient (mas (km s^{-1})$^{-1}$)	Gradient P.A. (°)	Zeeman Pair
				6035 MHz				
R	12.36	−883.778	707.787	0.201	0.25	...	...	A
L	12.61	−883.134	707.356	0.262	0.25	...	...	a
R	13.82	−855.931	698.986	2.499	0.31	1.40	132	B
L	14.06	−855.852	698.853	1.374	0.34	1.15	155	b
R	13.92	−847.432	691.329	0.405	0.17	...	...	C
R	15.16	−257.680	100.194	0.622	0.17	7.72	−70	D
L	15.42	−258.373	99.586	0.475	0.18	...	...	d
R	15.18	−250.056	102.927	1.276	0.26	1.48	−83	E
L	15.45	−250.018	103.112	0.824	0.26	2.09	−41	e
R	13.98	−227.783	102.493	0.195	0.20	...	...	F
L	14.28	−227.264	101.794	0.241	0.19	...	...	f
R	14.78	−202.760	87.994	0.229	0.24	...	...	G
L	15.07	−203.000	87.858	0.218	0.24	...	...	g
R	5.51	−128.465	994.596	2.229	0.26	1.16	−6	H
L	5.5[b]	−128.492	995.516	0.227	...	...	...	(h)
R	−0.20	−49.760	1013.784	2.241	0.27	1.09	−54	I
L	0.48	−49.883	1013.685	1.702	0.27	0.89	−12	i
R	−0.63	−47.799	1011.481	0.668	...	2.90	127	J
R	14.50	0.000	0.000	10.274	0.21	0.75	156	K[a]
L	14.79	0.148	−0.515	0.320	...	...	...	k
R	13.67	33.361	533.130	1.981	0.25	12.52	−68	L
L	13.76	33.598	533.325	0.919	0.26	8.60	−72	l
R	14.40	148.685	−0.352	0.583	0.20	...	...	M
L	14.47	147.241	0.679	0.446	0.22	...	...	m
R	14.43	160.529	−6.392	1.147	0.21	...	...	N
L	14.50	160.754	−6.787	0.976	0.22	4.81	130	n
				6030 MHz				
R	13.79	−855.753	699.107	3.244	0.28	1.11	169	Z[a]
L	14.12	−856.052	698.982	1.297	...	1.12	−124	z
L	13.81	−855.762	699.078	2.323	0.18	...	...	(z)

Notes. Positions are offsets as measured from $20^h10^m09^s.0768$, $+31°31'34''.923$ (J2000).
[a] Reference feature.
[b] Velocity cannot be determined to an additional significant digit. See the text.

Both the parallel-hand and cross-hand polarization correlations were obtained in order to reconstruct all Stokes quantities.

Data were reduced using the Astronomical Image Processing System (AIPS). The source 3C345 was used for instrumental delay and bandpass calibration, and J2136+0041 was used for polarization calibration. The polarization position angle of J2136+0041 was taken to be $-162°.68$ from the average of *C*-band entries in the Very Large Array (VLA)/Very Long Baseline Array (VLBA) Polarization Calibration Database.[3] Visibility weights were modified by taking their fourth roots in order to minimize the extent to which the overall calibration solutions would be dominated by the Effelsberg–GBT baseline (and baselines to these two highly sensitive telescopes). Since OH masers usually display substantial circular polarization, the ON 1 data were self-calibrated using one circular polarization of a bright maser spot in each transition, and the calibration solutions were applied to both polarizations.

The source J2003+3034 was used to determine the absolute position of a bright reference maser feature (listed in Table 1) at each of the two frequencies. Images were produced in all four Stokes parameters as well as both right and left circular polarizations (RCP and LCP, corresponding to RR and LL correlations). Maser spots were identified in the RR and LL cubes where emission was above six times the rms noise in each velocity channel. For each maser feature, spectra were obtained by integrating over a tight rectangular box encompassing the feature emission.

3. RESULTS

We detected 29 masers, of which the vast majority (26) are 6035 MHz masers (Table 1). The distribution of 6.0 GHz masers, shown in Figure 1, confirms at higher resolution the general distribution seen at lower resolution (Fish 2007). The spectra of recovered emission (total flux density in spots identified as masers) are shown in Figure 2. The spectra are very good qualitative matches to those obtained by Green et al. (2007).

Neither 6035 MHz masers at $v_{LSR} \approx +1$ or $+2$ km s^{-1} in the north of the source nor any low-velocity 6030 MHz masers are detected, despite their appearance in previous studies of ON 1 (Baudry et al. 1997; Fish et al. 2006; Fish 2007). These masers were weak (peak flux density 0.2 Jy, or approximately the flux density of the weakest detected maser in this work) in the Baudry et al. (1997) Effelsberg observations. At least one such maser was seen above a brightness level of 0.7 Jy beam^{-1} in the EVLA observations of Fish (2007), suggesting variability. We note a possible RCP 6035 MHz feature at (−164, +1049) mas, $v_{LSR} = +2.61$ km s^{-1} in our data, but the spot is seen

[3] http://www.vla.nrao.edu/astro/calib/polar

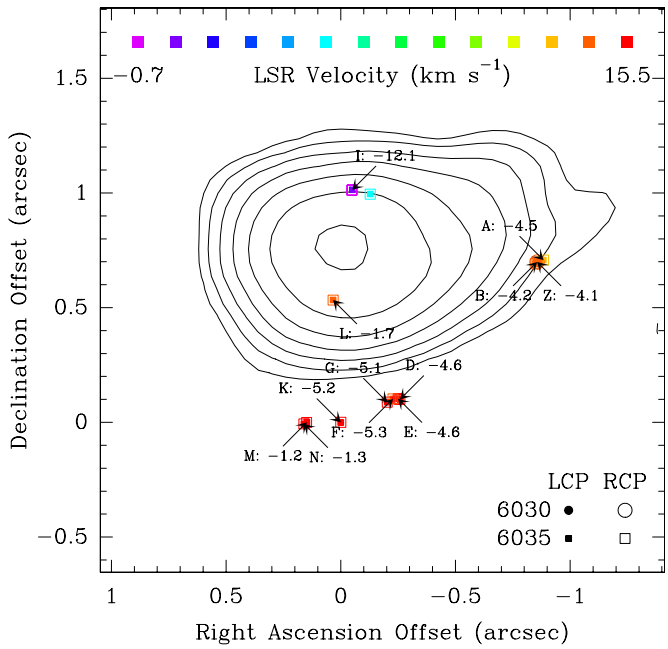

Figure 1. Map of 6.0 GHz masers in ON 1. Squares and circles denote 6035 MHz and 6030 MHz masers, respectively. Maser lines identified in RCP are shown as open symbols, while LCP masers are shown as filled symbols. Numbers indicate magnetic fields in milligauss as derived from Zeeman splitting, with letters denoting the associated features in Table 1. Contours show 8.4 GHz continuum emission (Argon et al. 2000). Offsets are measured from $20^{h}10^{m}09\overset{s}{.}0768$, $+31°31'34\overset{''}{.}923$ (J2000).

(A color version of this figure is available in the online journal.)

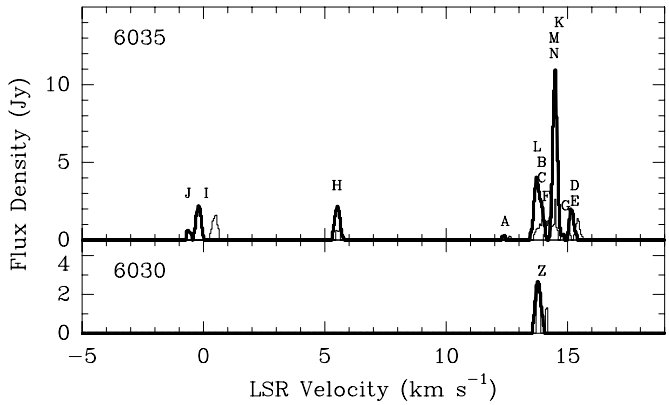

Figure 2. Total recovered maser emission in ON 1. RCP is shown in bold and LCP in normal weight. The same vertical scale is used for both panels. Letters denote features in Table 1.

only in one channel and only at 5.7σ, which does not meet our detectability criteria.

Nearly every 6030 and 6035 MHz maser feature is found with an accompanying feature in the opposite polarization at a slightly different velocity, presumably due to Zeeman splitting in the presence of a magnetic field. There are 12 or 13 readily identifiable Zeeman pairs constituting 24 or 26 maser spots. The high Zeeman pairing efficiency (over 80% of the detected 6 GHz masers can be paired) in the 6 GHz transitions is consistent with the small Zeeman splitting coefficients at 6030 and 6035 MHz as compared with the ground-state transitions. Observations of W3(OH) show a similar trend for increased Zeeman pairing efficiency with decreased Zeeman splitting in velocity units (Wright et al. 2004b; Fish & Sjouwerman 2007).

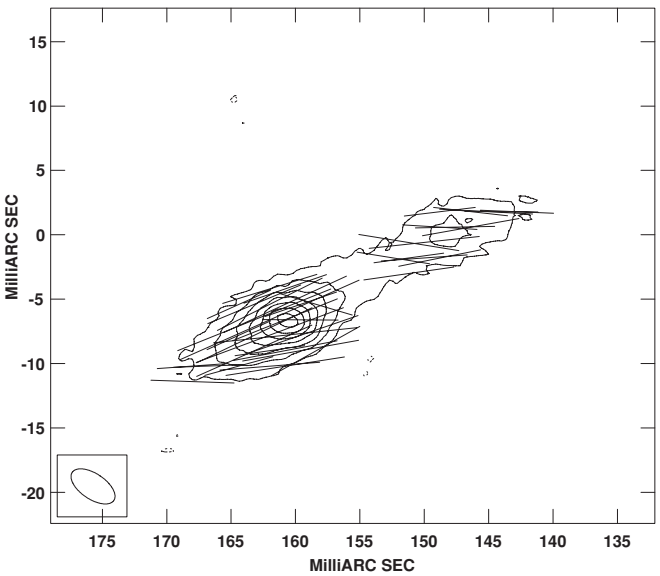

Figure 3. Integrated Stokes I emission and polarization of spots Mm and Nn in the velocity range 14.31–14.65 km s^{-1}. Contours are shown as multiples of 4 times the rms noise. Lines indicate the direction of linear polarization.

We detect linear polarization at the 4σ level or greater in several maser spots. At 6030 MHz, spot Z shows a linear polarization fraction ($\sqrt{Q^2+U^2}/I$) of 17% with an electric vector polarization angle of $-32°$ east of north in the channel of peak emission, approximately consistent with Green et al. (2007). At 6035 MHz, spot K is 22% linearly polarized with a position angle of 52° and spot B is 17% linearly polarized at $-19°$. There is evidence that the position angle of these spots may vary across the emission line in frequency. There is a ridge of weak emission in eight consecutive velocity channels passing through spots Mm and Nn. The linear polarization in spots Mm and Nn is not strong in any individual velocity channel, but after integrating over all eight velocity channels in which emission is detected in this region, linear polarization is clearly detected and found to be aligned with the ridge (Figure 3).

Positional gradients are computed via weighted least-squares fitting of a straight line to a maser spot's centroid right ascension and declination in each frequency channel in which it is detected. The positional gradients, given in Table 1, indicate the magnitude and position angle of the gradient (increasing in the direction of positive velocity). Maser components in Zeeman associations have similar positional gradients. It is possible that the very large gradient of spot Ll results from the spatial blending of two spots separated by less than the synthesized beamwidth. Blending of nearby maser spots can make it difficult to determine positional gradients when masers are not clearly isolated; for instance, the positional gradient of spot n is roughly aligned with the ridge of emission connecting it with spot m. Green et al. (2007) note a positional gradient aligned along a northwest–southeast direction in three of five 6035 MHz Zeeman pairs, although it is not clear from their text whether the ridge of spots Mm and Nn (which would have appeared as a single spot at their resolution) is one of them.

4. DISCUSSION

4.1. Zeeman Pairs

The LCP and RCP components of 6 GHz Zeeman pairs are found to have a very small spatial separation. The separation

Table 2
Multitransition Zeeman Associations

6.0 GHz Zeeman Group	6.0 GHz B (mG)	6.0 GHz Separation (mas)	6.0 GHz $v_{\rm LSR}^{\rm sys}$ (km s^{-1})[a]	1.6 GHz LCP R.A. Offset (mas)	1.6 GHz LCP Decl. Offset (mas)	1.6 GHz LCP $v_{\rm LSR}$ (km s^{-1})	1.6 GHz RCP R.A. Offset (mas)	1.6 GHz RCP Decl. Offset (mas)	1.6 GHz RCP $v_{\rm LSR}$ (km s^{-1})	1.6 GHz B (mG)[b]
A	−4.5	0.77	12.48	−884.60	707.53	13.75	...	...	...	−4.3
B	−4.2	0.15	13.94	−855.70	697.28	15.15	...	...	...	−4.1
Z[c]	−4.1	0.32	13.95							
D	−4.6	0.92	15.29	−258.85	100.60	16.73	−259.45	100.83	13.92	−4.8
E	−4.6	0.19	15.32	−249.24	102.42	16.73	−249.72	103.36	13.68	−5.2
F	−5.3	0.87	14.13	−233.76	97.58	16.35	...	...	...	−7.5
G	−5.1	0.28	14.92	−201.74	85.70	15.88	...	...	...	−3.2
H	...	0.92[d]	5.50	...	...	...	−128.22	994.63	5.95	+1.7
I	−12.1	0.10	0.14	−50.68	1012.23	3.90	...	...	...	−12.8
K	−5.2	0.54	14.64	...	...	...	−0.02	−0.02	12.82	−6.1[e]
L	−1.7	0.31	13.72	40.34	526.99	13.88	39.19	527.41	13.21	−1.1
N[f]	−1.3	0.45	14.47	154.58	−6.23	15.05	152.31	−4.82	14.02	−1.7[g]
				161.92[h]	−13.37	14.64	160.68[g]	−13.49	14.29	−1.0

Notes. The columns 6.0 GHz and 1.6 GHz refer to the 6035 MHz and 1665 MHz transitions, respectively, except as noted in the table. The 1.6 GHz maser information is taken from Table 2 in Fish & Reid (2007).
[a] Systemic velocity (corrected for Zeeman splitting).
[b] When two 1.6 GHz spots are given, magnetic field is as derived from 1.6 GHz Zeeman pair. When only one 1.6 GHz spot is given, magnetic field is inferred from multitransition overlap.
[c] 6030 MHz.
[d] Interpreting the RCP and LCP features as Zeeman components.
[e] Paired with a distant LCP feature to give a −2.5 mG field in Fish & Reid (2007).
[f] Spatially blended with Zeeman group M, which implies an almost identical magnetic field strength and systemic velocity.
[g] Alternatively, the 6035 MHz spots may be grouped with (162.13,−7.20) mas LCP 1665 MHz to give a −1.0 mG field.
[h] 1667 MHz.

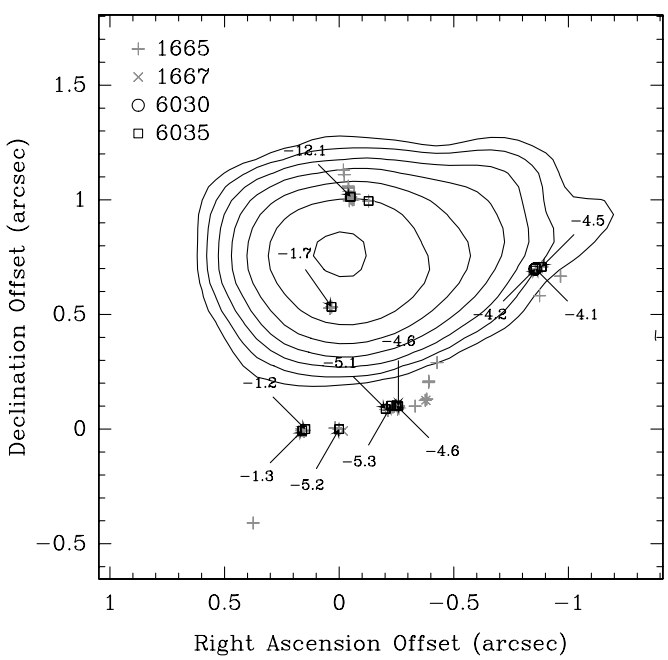

Figure 4. Relative locations of 6030/6035 MHz masers and ground-state masers (in gray; from Fish & Reid 2007). Adopted alignment of the two data sets is discussed in Section 4.2.

between the centroid positions of the peak channels of the LCP and RCP spots of a 6.0 GHz Zeeman pair does not exceed 1 mas except for the pair Mm, the weaker component of the aforementioned ridge of emission in the southeast. A Zeeman component is identified for every 6.0 GHz maser whose emission is not spatially blended with that of another, brighter spot. The two spots labeled Hh may constitute a Zeeman pair, but the weakness of the LCP feature prohibits measuring its velocity accurately enough to identify the magnetic field strength and direction.

Only one Zeeman pair was identified at 6030 MHz. It was found to be spatially coincident with another Zeeman pair at 6035 MHz to within a few tenths of a milliarcsecond. The magnetic field and unshifted velocity of the 6030 and 6035 MHz pairs agree to within 0.1 mG and 0.01 km s^{-1}, respectively. Our magnetic field strengths are broadly consistent with those of Desmurs & Baudry (1998). Differences on the order of 1–2 mG can be explained by the lower spectral resolution of the Desmurs & Baudry (1998) observations (0.11 km s^{-1} channel separation = 1.4 mG at 6030 and 2.0 mG at 6035 MHz). Our magnetic field measurements are highly consistent with the MERLIN observations of Green et al. (2007), with differences well under 1 mG (no greater than 0.2 mG in five of six Zeeman pairs).

4.2. Multitransition Maser Associations

We find that nearly every 6.0 GHz maser detected in ON 1 is found in close (i.e., less than 10 mas) association with at least one ground-state maser spot (Figure 4) when the brightest 6035 MHz spot is aligned with the brightest 1665 MHz spot detected by Fish & Reid (2007). This result differs from the results of Green et al. (2007), who find from lower-resolution MERLIN data that the closest 6.0/1.6 GHz separation involves a peak separation of 28 mas. Fish & Reid (2007) did not obtain absolute positions for the 1665 and 1667 MHz masers; nevertheless the separations between the 6.0 GHz and nearest 1.6 GHz masers listed in Table 2 are always within a few milliarcseconds, and at least one associated ground-state maser can be found for almost every 6.0 GHz maser found in this work.

The close spatial associations allow for multitransition Zeeman associations to be identified. The Zeeman effect shifts LCP and RCP components in frequency by the magnetic

field strength multiplied by a constant splitting factor that is different for each transition. Under the assumption that multitransition associations are produced by the same cloudlets of material, the magnetic field strength and systemic velocity can be derived so long as any two Zeeman components can be identified from among all transitions seen in spatial overlap. Table 2 lists the magnetic fields derived from Zeeman associations including both 6.0 GHz and 1.6 GHz masers. There are four Zeeman associations in which a complete Zeeman pair is found at both 6035 MHz and 1665 MHz (and one additional pair at 1667 MHz). The magnetic fields obtained in these transitions are consistent with each other in all cases to 0.6 mG or better. The excellent agreement between magnetic field strengths obtained from 1.6 GHz Zeeman pairs and 6.0 GHz Zeeman pairs provides strong evidence supporting the alignment between the reference frames of these observations and the Fish & Reid (2007) VLBA observations.

Furthermore, Zeeman associations consisting of a pair of LCP and RCP components at 6030 MHz and a single unpaired component at 1665 MHz show that the implied magnetic field at 1665 MHz (assuming that the systemic velocity is given by the average of the 6035 MHz LCP and RCP velocities) is consistent with the 6035 MHz value. In the six such associations, the maximum difference between the 6035 MHz and implied 1665 MHz magnetic fields is 2.2 mG, with four associations showing a difference of less than 1 mG. We refer to these instances as "multitransition Zeeman associations" and argue that the above results support the validity of using these to derive magnetic fields.

Of note is a potential +1.7 mG magnetic field implied by the overlap of a 6035 MHz RCP spot (H) with a 1665 MHz RCP spot at a different velocity. There is also a very weak 6035 MHz LCP spot (h) at this position whose velocity cannot be determined to sufficient accuracy to identify the sign of the magnetic field from the 6035 MHz Zeeman pair alone.

There does not appear to be a significant correlation between the brighter polarization at 6035 MHz and that in a nearby ground-state transition, usually 1665 MHz. When the flux ratio between Zeeman components at 6035 MHz is close to unity ($\lesssim$2.5), there is no correlation at all. Only two 6035 MHz Zeeman pairs have a component flux ratio greater than 2.5: Hh and Kk. In both instances, the brighter Zeeman component at 6035 MHz is RCP, and the RCP feature at 1665 MHz is detected, but the LCP feature is not (Fish & Reid 2007). In the one case where a 6030 and 6035 MHz spot overlap, the RCP component is brighter than the LCP component in both transitions, and the RCP/LCP ratio is greater for the 6030 MHz transition. (However, emission at 1665 MHz which is spatially coincident with these Zeeman pairs is seen only in LCP, not RCP.) There is also one instance where the 1665, 1667, and 6035 MHz masers overlap, and the Zeeman component flux ratios decrease in that order. This is consistent with the flux ratios varying monotonically with the Zeeman splitting ratio (Wright et al. 2004b). There is also a similar trend for 6.0 GHz Zeeman pairs to have smaller *separation* between LCP and RCP components than is seen for coincident ground-state transitions (an effect also noted in W3(OH) by Fish & Sjouwerman 2007) in W3(OH). These effects may be related if, for instance, excitation conditions (such as velocity coherence) change slightly over the physical extent of a Zeeman association.

The large number of Zeeman pairs identified in transitions of OH allows a systemic maser velocity map of ON 1 to be constructed, as shown in Figure 5. Hydroxyl maser velocities

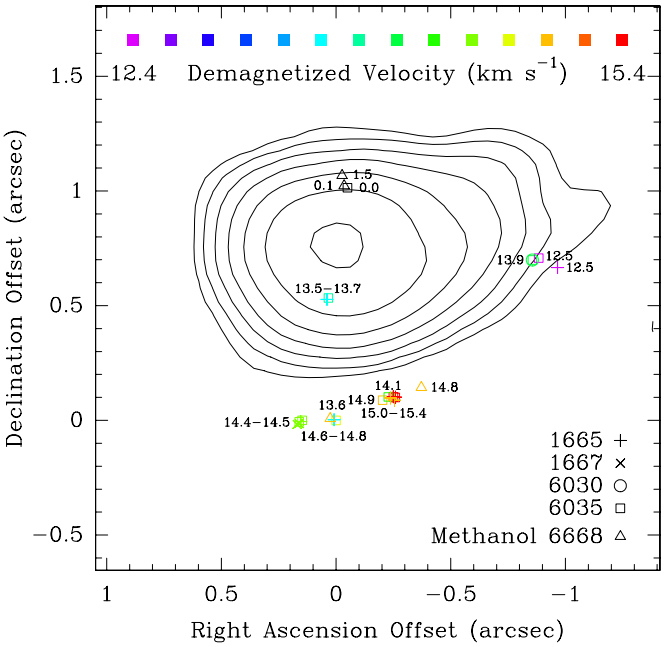

Figure 5. LSR velocities corrected for Zeeman splitting. Color indicates the central (unshifted) velocity for Zeeman pairs in each transition (also indicated with numbers), with northern masers ($v_{\rm LSR} \ll 12.4$ km s^{-1}) in black. Multitransition Zeeman associations are not shown. Methanol maser data is taken from Rygl et al. (2010).

(A color version of this figure is available in the online journal.)

have been corrected for Zeeman splitting, which can be large (several km s^{-1} between LCP and RCP components) in the ground state. Methanol maser positions from Rygl et al. (2010) and Xu et al. (2009) are included. No such correction is required for methanol, which is a nonparamagnetic molecule. There is a trend for LSR velocities to increase toward the west along the southern line of maser spots, although not all Zeeman pairs and methanol masers conform to this pattern.

4.2.1. Alignment of Maser Positions

In aligning the 6.0 GHz masers with the Fish & Reid (2007) 1.6 GHz masers, we note that there is no particular reason to believe that the position of the brightest 6035 MHz will be precisely coincident with the location of the brightest 1665 MHz maser to submilliarcsecond accuracy. The apparent centroids of Zeeman components may appear at slightly different locations. For instance, the separation between the components of 6.0 GHz Zeeman pairs listed in Table 2 is typically a few tenths of a milliarcsecond. This effect is even larger at 1665 and 1667 MHz, where the separation between components of a Zeeman pair can be a few milliarcseconds. Assuming that there is no large-scale organization that systemically shifts LCP spots in one direction and RCP spots in the opposite direction, we can define a best statistical alignment of the 6.0 and 1.6 GHz maser frames by finding the single vector (right ascension and declination) offset to add to the positions of one of the frames to minimize the sum of the squares of the 6.0 GHz–1.6 GHz position differences among the Zeeman associations. We use the data in Table 2, using the average of RCP and LCP positions within one frequency as the central location of the maser emission at that frequency in each Zeeman association. When only one sense of circular polarization is detected in a Zeeman association in a frequency, we use that position as the assumed central location of the maser emission at that frequency. We find that

the two frames are best aligned when the 1665 MHz reference feature of Fish & Reid (2007) is assumed to be 1.7 mas north of the 6035 MHz reference feature. In this frame, the median 1.6/6.0 GHz offset in the Zeeman associations is approximately 2.2 mas.

The offsets between 1.6 and 6.0 GHz Zeeman associations are consistent in magnitude with proper motions of masers in ON 1. The Fish & Reid (2007) data were observed 3.74 yr prior to the epoch of observations of the 6.0 GHz masers reported here. A 1.7 mas apparent offset between the epochs could correspond to a motion of 5.5 km s^{-1} at a distance of 2.57 kpc (Rygl et al. 2010). This is comparable to the 1.6 GHz maser motions seen in Fish & Reid (2007). Although the lack of phase referencing in the ground-state observations precludes rigorous analysis of the offsets in terms of proper motions, the general pattern is confirmed by the 6.7 GHz methanol observations of Rygl et al. (2010), which show that the relative speed of the northern and southern methanol masers in the plane of the sky is 9.4 km s^{-1}.

4.3. Comparison with W3(OH)

It is instructive to compare ON 1 with W3(OH), the other massive star-forming region hosting a large number of 6.0 GHz masers observed with a modern VLBI array. There are numerous similarities between the properties of 6.0 GHz masers in ON 1 and W3(OH), some of which have already been commented on in Sections 3 and 4. For instance, 6030 MHz masers in ON 1 are rare and are only found in the presence of 6035 MHz masers. This is consistent with observations of W3(OH), which found that 6030 MHz masers are nearly always found in close spatial association with 6035 MHz masers and imply similar physical conditions (Fish & Sjouwerman 2007).

However, one important contrast between the OH masers in ON 1 and W3(OH) is that in the former, all 6035 MHz masers are found in close association with 1665 MHz masers. This stands in stark contrast with W3(OH), where many 6035 MHz maser spots are found without accompanying ground-state emission, including some (particularly in the NE and SE regions) where no ground-state masers are located within hundreds of AU (Fish & Sjouwerman 2007). Theoretical modeling suggests that co-propagation of 1665 and 6035 MHz masers (as observed throughout ON 1) can occur under a wide range of conditions, but the presence of 6035 MHz masers without 1665 MHz masers may require a higher density and/or higher OH column density (e.g., Gray et al. 1992; Cragg et al. 2002). It is therefore probable that the OH masers in ON 1 are on the whole tracing slightly less dense material than in W3(OH).

Collisions may also play a partial role in exciting the 6035 MHz transition (Gray et al. 1992). It is possible, for instance, that the masers just south of the H II region trace a shock front. The appearance of ground-state, satellite-line masers in this region (Nammahachak et al. 2006) may also be indicative of a shock (Gray et al. 1992; Pavlakis & Kylafis 1996a, 1996b).

Methanol maser excitation is predicted to occur over a similar range of densities (Cragg et al. 2002). The tentative detection of a magnetic field strength of −18 mG in methanol Zeeman splitting by Green et al. (2007) may be indicative of a slightly higher density locally at the methanol maser site in the southern line of masers in ON 1. Methanol emission is also seen intermixed with OH masers in W3(OH) (Harvey-Smith & Cohen 2006).

In W3(OH), 31% of the 6.0 GHz masers are 6030 MHz masers, which are typically weaker than their 6035 MHz maser counterparts by a factor of several (Fish & Sjouwerman 2007). In ON 1, only 10% of the 6.0 GHz masers are in the 6030 MHz transition. This may not be a significant difference, due both to the smaller number of total maser spots in ON 1 and the fact that the 6.0 GHz masers are weaker than in W3(OH), meaning that a larger fraction of the presumed 6030 MHz maser population in ON 1 may be below our detectability threshold. The modeling of Pavlakis & Kylafis (2000) and Cragg et al. (2002) shows that the parameter spaces under which 6030 and 6035 MHz masers are likely to be excited in star-forming regions are very similar. For identical excitation conditions (as would occur if 6030 and 6035 MHz masers were found in spatial overlap), Cragg et al. (2002) find that the brightness temperature of the 6030 MHz is typically a factor of a few smaller than that of the 6035 MHz maser. However, 6030 MHz masers are found only in the west, despite the fact that all maser clusters in ON 1 (northern, central, western, and the line of masers in the south) host 6035 MHz masers that are at least a factor of 10 brighter than our detection threshold. It is not clear what, if any, are the differences among the physical conditions of these clusters that allow 6030 MHz maser formation only in the west.

4.4. The Structure of ON 1

The view of ON 1 has evolved with increasingly better observational data. Israel & Wootten (1983) suggested that ON 1 was an example of isolated massive (spectral type B0.5) star formation. More recent infrared (Kumar et al. 2002, 2003, 2004), centimeter, and submillimeter observations (Su et al. 2004, 2009) indicate that the environment of ON 1 contains numerous dust cores associated with other intermediate-mass or high-mass star formation. Multiple molecular outflows and high-velocity water maser structures add further complexity to the surroundings of the H II region, suggesting that the source(s) in the H II region are gravitationally bound to other nascent and possibly evolved stars in the region (Nagayama et al. 2008; Su et al. 2009). The complicated environment of ON 1 renders it difficult to interpret the OH masers surrounding the H II region.

Nevertheless, based on the OH maser distribution in multiple transitions, it is likely that the H II region is associated with at least two distinct excitation sources. The highly excited 13,441 MHz transition of OH produces masers near both 0 and 14–15 km s^{-1} (Baudry & Desmurs 2002; Fish et al. 2005). Archival VLBA observations (experiment code BB137) of this transition were unsuccessful in detecting the emission, so no interferometric map of the 13,441 MHz masers exists. However, VLBI maps of 6.7 GHz methanol masers, which show a similar double-peaked spectrum at 0 and 14–15 km s^{-1}, are consistent with emission in the northern and southern groups (Sugiyama et al. 2008; Rygl et al. 2010; see also Green et al. 2007), as shown in Figure 5. The existence of a 12 mG magnetic field, large for OH masers, in the north argues that the northern masers (Hh, Ii, and J) are located close to one of these excitation sources. The magnetic field measurements in the south are less conclusive, although if the −18 mG magnetic field inferred from methanol Zeeman splitting (Green et al. 2007) is correct, the bright 6035 MHz reference feature (K) may be located closest to the southern excitation source. We note the possibility, however, that the large magnetic field strengths and existence of highly excited OH masers in the north and south may simply be due to dense molecular clumps on opposite sides of an H II region containing only one excitation source.

The southern masers, which constitute the bulk of the observed OH masers in ON 1, are probably best understood in the context of the Elitzur & de Jong (1978) model of OH masers forming in the compressed region between the ionization and

shock fronts around an expanding H II region. These masers appear at the edge of the H II region as observed at $\lambda = 1.3$ cm and are located not too far from the edge of the dust cavity evacuated by the H II region (Su et al. 2009). The systemic velocity of the molecular cloud is fairly well established to be $v_{\rm LSR} = 11$–12 km s^{-1} from a large variety of dense molecular tracers including ammonia, formaldehyde, CS, SiO, thermal methanol, and Class I methanol masers (e.g., Haschick & Baan 1989; Haschick & Ho 1990; Haschick et al. 1990; Plume et al. 1992; Anglada et al. 1996; MacLeod et al. 1998; Kalenskiĭ et al. 2001; Araya et al. 2002). The line-of-sight velocity of the southern masers is close to the assumed systemic dust velocity of 11–12 km s^{-1} but slightly redshifted (Figure 5), with the offset from systemic ranging from less than 1 to over 3 km s^{-1}. This (line-of-sight) velocity offset is consistent in magnitude with the 3.6 km s^{-1} (transverse) proper motion inferred by Rygl et al. (2010) from methanol maser observations and the expansion of the H II region. Unfortunately, the linear polarization in this region (from this work as well as Fish et al. 2005 and Green et al. 2007) is complicated enough to prevent definitive identification of the large-scale magnetic field direction in the plane of the sky along the line of southern masers.

The northern masers are associated with the largest magnetic field strength seen in the source (-12 mG at spots Ii). More so than in other maser clumps, the northern masers divide neatly into regions where only the LCP component is seen at 1665 MHz and regions where the RCP component is seen. After the reference feature, the 6035 MHz Zeeman association with the largest component flux ratio is located in the northern cluster. These features may be explainable by correlated magnetic fields and velocity gradients (Cook 1966) or by Zeeman overlap (Deguchi & Watson 1986). There is also a relative dearth of linear polarization in this region, at both 6035 MHz and 1665 MHz (Fish et al. 2005). Indeed, the Zeeman splitting from the large magnetic field at spot Ii is larger than the maser line width, which is predicted by Zeeman overlap to produce masers that are very highly circularly polarized (Deguchi & Watson 1986).

Understanding the northern masers may require understanding both the multiplicity of massive stars in the H II region and the velocity of the H II region. Zheng et al. (1985) measured the velocity to be +5 km s^{-1} at 14.7 GHz, although there is a reason to believe that this velocity may be significantly blueshifted from the systemic velocity of the massive star(s) in the H II region due to optical depth effects in the expanding plasma (see discussion in Fish & Reid 2007), which are visible in the $\lambda = 3.6$ and 1.3 cm continuum maps of Su et al. (2009). Three possibilities arise: the Zheng et al. (1985) velocity may indeed trace the velocity of a single massive star within the H II region; there may be only one excitation source in the H II region, but its velocity is not given by the 14.7 GHz recombination line; or there may be more than one excitation source within the H II region.

In the first case, if there is only one source of excitation at $v_{\rm LSR} \approx +5$ km s^{-1}, the northern and southern masers are presumably both associated with it. In this case, the interpretation of Fish & Reid (2007) is probably correct: maser motions are dominated by the expansion of the ionized region and an additional rotational component, each having a magnitude of several km s^{-1}. As is usual in massive star-forming regions, not all OH maser velocities fit nicely into the large-scale velocity pattern, but it is plausible that the differences can be explained by projection effects and inhomogeneities in the density profile of the molecular material.

In the second case, the systemic velocity of the ON 1 system, given by the presumed lone massive star inside the H II region, is likely close to the systemic molecular velocity of 11–12 km s^{-1}. Recombination line studies of other ultracompact H II regions show that centimeter-wavelength recombination lines are typically blueshifted compared to millimeter-wavelength recombination lines (see discussion in Section 3.3 of Sewilo et al. 2008). Since the optical depth of the H II region decreases with frequency, higher-frequency recombination lines are sensitive to the center of the H II region (where the massive star is likely located), while lower-frequency lines trace the expanding outer portions of the H II region and are therefore blueshifted (Berulis & Ershov 1983; Welch & Marr 1987; Keto et al. 1995). If the same effect operates in ON 1, the velocities of the northern masers (mostly near 0 km s^{-1}) differ by more than 10 km s^{-1} from the rest of the OH masers, the systemic velocity of the molecular material in the vicinity, and presumably the velocity of the star in the center of the H II region. It is possible, then, that the northern masers trace an outflow, possibly with a helical magnetic field. Ground-state RCP and LCP features have a tendency to segregate on opposite sides of the presumed structure, which could be explained if the magnetic field wraps around the outflow. Unfortunately, the magnetic field direction and strength at spot Hh are poorly determined due to the low signal-to-noise ratio of the LCP spot, so it is not possible to confirm that the polarity of the magnetic field reverses across the northern structure.

In the third case, there are at least two massive stars in the H II region, each with associated OH masers. The Zheng et al. (1985) recombination line velocity may represent an average of the velocities of the two sources, although optical depth effects may still be important. Based on both the recombination line velocity and the fact that the northern masers (unlike the southern masers) are projected atop the H II region, it is probable that the northern excitation source is in front of the southern excitation source. Either the expansion/rotation or outflow interpretation of the maser distributions may apply, depending on the relative velocities of the two excitation sources.

In contrast with observations of W3(OH), the 6.0 GHz masers in ON 1 do not clearly trace additional structures that were not visible at 1.6 GHz, limiting their ability to provide additional information on the context of the various maser clusters in the source. Further understanding of how the maser clusters are associated with one another will require higher-resolution observations of the nonmasing material. Sensitive observations of high-frequency recombination lines in the H II region may be illuminating regarding the internal structure of the ionized region, especially if done with enough spatial resolution to understand the internal dynamics of the ionized region. ALMA observations of dense molecular tracers may also assist in providing the context in which star formation is taking place in ON 1.

5. CONCLUSIONS

We have imaged the 6030 and 6035 MHz OH masers in ON 1 at VLBI resolution. The distribution of these excited-state masers is similar to that of the ground-state masers. Unlike in the similar massive star-forming region W3(OH), 6.0 GHz masers are not found in the absence of 1665 MHz masers, perhaps suggesting that ON 1 does not have analogues of the highest-density knots found in W3(OH). The 6.0 GHz masers are spatially coincident with 1665 MHz masers to within a

few milliarcseconds. Magnetic fields strengths obtained from Zeeman splitting at 6.0 and 1.6 GHz are usually consistent to better than 1 mG, suggesting that multitransition Zeeman associations are acceptable for obtaining estimates of the local magnetic field.

Our observations confirm the existence of a strong (−12 mG) magnetic field among the northern, blueshifted masers, as suspected from early EVLA observations of ON 1 (Fish 2007). The large magnetic field here, as well as the distribution of methanol maser spots and presumed distribution of the highly excited 13,441 MHz OH masers, may indicate that the northern and southern masers are excited by two different sources within the H II region or that the northern masers trace and outflow. However, other scenarios, such as large-scale expansion and rotation of all groups of masers in ON 1, cannot be ruled out from the data at hand. The overall structure of ON 1 remains uncertain in the absence of sensitive, high-resolution observations of the nonmasing material.

The National Radio Astronomy Observatory is a facility of the National Science Foundation operated under cooperative agreement by Associated Universities, Inc. The European VLBI Network is a joint facility of European, Chinese, South African, and other radio astronomy institutes funded by their national research councils.

Facilities: EVLA, EVN, GBT

REFERENCES

Anglada, G., Estalella, R., Pastor, J., Rodriguez, L. F., & Haschick, A. D. 1996, ApJ, 463, 205
Araya, E., Hofner, P., Churchwell, E., & Kurtz, S. 2002, ApJS, 138, 63
Argon, A. L., Reid, M. J., & Menten, K. M. 2000, ApJS, 129, 159
Baudry, A., & Desmurs, J. F. 2002, A&A, 394, 107
Baudry, A., Desmurs, J. F., Wilson, T. L., & Cohen, R. J. 1997, A&A, 325, 255
Berulis, I. I., & Ershov, A. A. 1983, Sov. Astron. Lett., 9, 341
Bloemhof, E. E., Reid, M. J., & Moran, J. M. 1992, ApJ, 397, 500
Cook, A. H. 1966, Nature, 211, 503
Cragg, D. M., Sobolev, A. M., & Godfrey, P. D. 2002, MNRAS, 331, 521
Deguchi, S., & Watson, W. D. 1986, ApJ, 300, L15
Desmurs, J. F., & Baudry, A. 1998, A&A, 340, 521
Elitzur, M., & de Jong, T. 1978, A&A, 67, 323
Fish, V. L. 2007, ApJ, 669, L81
Fish, V. L., & Reid, M. J. 2007, ApJ, 670, 1159
Fish, V. L., Reid, M. J., Argon, A. L., & Zheng, X.-W. 2005, ApJS, 160, 220
Fish, V. L., Reid, M. J., & Menten, K. M. 2005, ApJ, 623, 269
Fish, V. L., Reid, M. J., Menten, K. M., & Pillai, T. 2006, A&A, 458, 485
Fish, V. L., & Sjouwerman, L. O. 2007, ApJ, 668, 331
Gardner, F. F., & Martin-Pintado, J. 1983, A&A, 121, 265
Gray, M. D., Field, D., & Doel, R. C. 1992, A&A, 262, 555
Green, J. A., Richards, A. M. S., Vlemmings, W. H. T., Diamond, P., & Cohen, R. J. 2007, MNRAS, 382, 770
Harvey-Smith, L., & Cohen, R. J. 2006, MNRAS, 371, 1550
Haschick, A. D., & Baan, W. A. 1989, ApJ, 339, 949
Haschick, A. D., & Ho, P. T. P. 1990, ApJ, 352, 630
Haschick, A. D., Menten, K. M., & Baan, W. A. 1990, ApJ, 354, 556
Ho, P. T. P., Vogel, S. N., Wright, M. C. H., & Haschick, A. D. 1983, ApJ, 265, 295
Israel, F. P., & Wootten, H. A. 1983, ApJ, 266, 580
Kalenskiĭ, S. V., Slysh, V. I., Val'Tts, I. E., Winnberg, A., & Johansson, L. E. 2001, Astron. Rep., 45, 26
Keto, E. R., Welch, W. J., Reid, M. J., & Ho, P. T. P. 1995, ApJ, 444, 765
Kumar, M. S. N., Bachiller, R., & Davis, C. J. 2002, ApJ, 576, 313
Kumar, M. S. N., Davis, C. J., & Bachiller, R. 2003, Ap&SS, 287, 191
Kumar, M. S. N., Tafalla, M., & Bachiller, R. 2004, A&A, 426, 195
MacLeod, G. C., Scalise, E. J., Saedt, S., Galt, J. A., & Gaylard, M. J. 1998, AJ, 116, 1897
Nagayama, T., Nakagawa, A., Imai, H., Omodaka, T., & Sofue, Y. 2008, PASJ, 60, 183
Nammahachak, S., Asanok, K., Hutawarakorn Kramer, B., Cohen, R. J., Muanwong, O., & Gasiprong, N. 2006, MNRAS, 371, 619
Pavlakis, K. G., & Kylafis, N. D. 1996a, ApJ, 467, 300
Pavlakis, K. G., & Kylafis, N. D. 1996b, ApJ, 467, 309
Pavlakis, K. G., & Kylafis, N. D. 2000, ApJ, 534, 770
Plume, R., Jaffe, D. T., & Evans, N. J., II 1992, ApJS, 78, 505
Rygl, K. L. J., Brunthaler, A., Reid, M. J., Menten, K. M., van Langevelde, H. J., & Xu, Y. 2010, A&A, 511, A2
Sewilo, M., Churchwell, E., Kurtz, S., Goss, W. M., & Hofner, P. 2008, ApJ, 681, 350
Su, Y.-N., Liu, S.-Y., & Lim, J. 2009, ApJ, 698, 1981
Su, Y.-N., et al. 2004, ApJ, 616, L39
Sugiyama, K., Fujisawa, K., Doi, A., Honma, M., Kobayashi, H., Bushimata, T., Mochizuki, N., & Murata, Y. 2008, PASJ, 60, 23
Welch, W. J., & Marr, J. 1987, ApJ, 317, L21
Wright, M. M., Gray, M. D., & Diamond, P. J. 2004a, MNRAS, 350, 1253
Wright, M. M., Gray, M. D., & Diamond, P. J. 2004b, MNRAS, 350, 1272
Xu, Y., Voronkov, M. A., Pandian, J. D., Li, J. J., Sobolev, A. M., Brunthaler, A., Ritter, B., & Menten, K. M. 2009, A&A, 507, 1117
Zheng, X. W., Ho, P. T. P., Reid, M. J., & Schneps, M. H. 1985, ApJ, 293, 522